



## Low-temperature quantum correction to anisotropic magnetoresistance in $\text{Tm}_3\text{Fe}_5\text{O}_{12}/\text{Pt}$ heterostructures

Zhiqiang Zhu, Xiaoguang Xu <sup>\*</sup>, Mengxi Wang, Chexin Li, Lu Cheng, Kangkang Meng,<sup>\*</sup>  
Yong Wu, Jikun Chen, Jun Miao, and Yong Jiang<sup>\*</sup>

*School of Materials Science and Engineering, University of Science and Technology Beijing, Beijing 100083, China*

 (Received 27 December 2021; revised 27 April 2022; accepted 13 May 2022; published 27 May 2022)

Spin transport in ferromagnetic insulator/heavy metal heterojunctions has attracted much attention because of its rich physics and potential applications. Here, we report an anomalous anisotropic magnetoresistance (AMR) at low temperature in a  $\text{Tm}_3\text{Fe}_5\text{O}_{12}/\text{Pt}$  bilayer, which has often been neglected for its weak signal compared with spin Hall magnetoresistance. In our study, the magnetic proximity effect is weak above 50 K so that the AMR signal is mainly caused by ordinary magnetoresistance and spin-related scattering. However, at low temperatures, the AMR changes dramatically due to the weak localization (WL) and weak anti-localization (WAL) related to the quantum diffusion mechanism. Moreover, the dominated mechanism changes from WL to WAL in a Cu-inserted structure of  $\text{TmIG}/\text{Cu}/\text{Pt}$  without the magnetic proximity exchange coupling at the interfaces, accompanied by an AMR variation from negative to positive. Our study reveals the quantum correction effect on the AMR, which provides a possible explanation of the complex resistive behavior at low temperatures.

DOI: [10.1103/PhysRevB.105.184428](https://doi.org/10.1103/PhysRevB.105.184428)

### I. INTRODUCTION

Magnetic insulators (MIs) are a type of material that allows the transport of spin current but not charge current. One type of MI is ferrimagnetic garnets, such as  $\text{Y}_3\text{Fe}_5\text{O}_{12}$  (YIG) and  $\text{Tm}_3\text{Fe}_5\text{O}_{12}$  (TmIG). YIG was extensively studied for its low damping and large magnon diffusion length to generate and transport pure spin current with minimal dissipation [1–4]. Compared with YIG, TmIG has also been widely studied due to its perpendicular magnetic anisotropy (PMA) [5–7]. However, a ferrimagnetic insulator/heavy metal (FI/HM) bilayer structure is necessary to detect the magnetic state of the FI layer. In the HM layer, the significant spin-orbit interaction usually results in large spin Hall effect (SHE) and inverse spin Hall effect (ISHE) [8–10], which can accomplish the conversion between charge current and transverse spin current. These two effects together lead to spin Hall magnetoresistance (SMR) [11–18]. Given that the magnitude of SMR is related to the angle between the spin-polarization direction of the spin current generated by the SHE in the HM and the magnetic-moment direction of the FI layer, SMR is a type of angular-dependent magnetoresistance (ADMR).

Anisotropic magnetoresistance (AMR) [19,20] is another type of ADMR and was first reported in ferromagnetic metals (Fe and Ni) in 1857 by Thomson *et al.* [21]. AMR is the magnetoresistance (MR) of magnetic materials depending on the angle between the directions of current and magnetization. In FI/HM bilayers, such as YIG/Pt, the AMR signal is

negligible at room temperature [12,15] and increases at low temperatures because of the magnetic proximity effect (MPE) [22–27]. Interestingly, an unusual AMR signal comparable to the magnitude of SMR was found in the YIG/Pt bilayer structure at low temperatures, which was ascribed to the emergence of weak anti-localization (WAL) [28]. However, the detailed study is limited and the mechanism needs to be further investigated.

Weak localization (WL) and WAL originate from the quantum diffusion and result in a correction to the conductance [29–34]. In the process of electron transport in solids, the quantum diffusion mechanism means that the electron can maintain its phase even after being scattered multiple times when its phase coherence length  $l_\phi$  is much larger than its mean free path  $l$ . According to this mechanism, the quantum interference between the time-reversed scattering closed loops will correct the conductance, which becomes more obvious with increasing  $l_\phi$  at lower temperatures. Apart from this, the correction is also sensitive to magnetic field because it can break the phase coherence, especially in materials with strong spin-orbit coupling. Because of this, an analysis of low-temperature MR curves has been launched to provide quantitative information about WL and WAL. The manipulation of the competition between WL and WAL has been widely studied in recent years, such as gate-voltage control in  $(\text{Bi}_x\text{Sb}_{1-x})_2\text{Te}_3$  [35], magnetic doping in  $\text{Bi}_2\text{Se}_3$  [36], and magnetism inducing via MPE in  $\text{Bi}_2\text{Se}_3/\text{FI}$  (YIG or TmIG) bilayers [37].

In this work, we employ a TmIG/Pt heterojunction to figure out how WL and WAL influence its AMR at low temperatures. To eliminate the MPE effect, we also design a series of samples by inserting a Cu layer with different thickness between the TmIG and Pt layers. It is found that both WL and

<sup>\*</sup>xgxu@ustb.edu.cn; kkmeng@ustb.edu.cn;  
yjiang@ustb.edu.cn

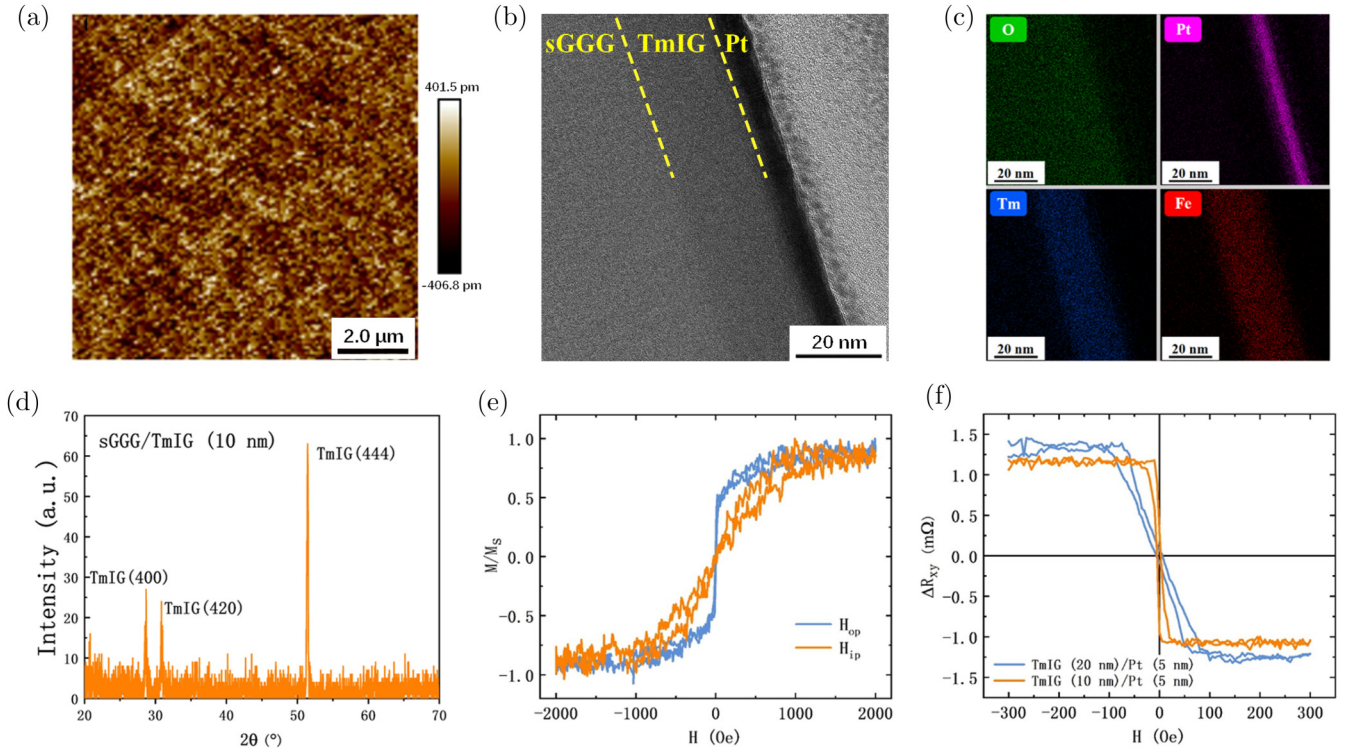


FIG. 1. (a) The AFM image ( $1\ \mu\text{m} \times 1\ \mu\text{m}$ ) of a TmIG (20) film. (b) The TEM image of the TmIG (20)/Pt (5) bilayer. (c) The EDS for O, Pt, Tm, and Fe elements mapping corresponding to panel (b). (d) GIXRD pattern of the TmIG (10) film grown on sGGG (111). (e) The in-plane and out-of-plane magnetic hysteresis loops of the TmIG (10)/Pt (5) sample at room temperature. (f) The anomalous Hall resistance loops for the TmIG/Pt samples at room temperature (the linear normal Hall resistance has been subtracted).

WAL play important effects on AMR when the temperature decreases. Moreover, the MPE at the TmIG/Pt interface may determine the change from WAL to WL.

## II. EXPERIMENTS

TmIG films with thicknesses from 5 to 20 nm were grown by using pulsed laser deposition (PLD) on sGGG[(Gd<sub>2.6</sub>Ca<sub>0.4</sub>)(Ga<sub>4.1</sub>Mg<sub>0.25</sub>Zr<sub>0.65</sub>O)<sub>12</sub>] (111) substrates at 750 °C and an oxygen pressure of 10 Pa with a repetition of 5 Hz, and then cooled down at a speed of 10 °C/min to room temperature. On the top of the TmIG films, a Pt (5) (thickness in nanometer) layer or Cu (2, 4, or 6)/Pt (5) bilayer was deposited by magnetron sputtering, with a base pressure better than  $3 \times 10^{-5}$  Pa. During the deposition, the Ar pressure was kept at 0.4 Pa. All samples were patterned into Hall bars with lateral dimensions of  $6\ \mu\text{m} \times 12\ \mu\text{m}$  by using electron beam lithography (EBL) and Ar ion milling.

The crystal structure and roughness of the TmIG (10) film were verified by grazing incidence x-ray diffraction (GIXRD, Rigaku D/max-2550) and atomic force microscopy (AFM, Bruker Icon). The TmIG/Pt bilayers were characterized by transmission electron microscopy (TEM, Jeol JEM-F200) and energy dispersive spectrometry (EDS, Jeol JEM-F200). The magnetic properties were measured using vibrating sample magnetometer (VSM, Quantum Design VersaLab) at room temperature. The magnetotransport measurements were carried out on Physical Property Measurement System (PPMS, Quantum Design DynaCool) between 1.8 and 300 K.

## III. RESULTS AND DISCUSSION

The surface of a TmIG (20) film was tested by AFM and the image ( $1\ \mu\text{m} \times 1\ \mu\text{m}$ ) is presented in Fig. 1(a). The surface of the TmIG film is smooth with a roughness of about 0.8 nm. The TEM image of TmIG (20)/Pt (5) in Fig. 1(b) demonstrates the clear layered structure of sGGG/TmIG/Pt. The EDS mapping in Fig. 1(c) shows the distribution of the O, Pt, Tm, and Fe elements, which is consistent with Fig. 1(b). The crystal structure of the TmIG (10) film was studied by GIXRD with the grazing angle of 1°. As shown in Fig. 1(d), three sharp peaks appear clearly, corresponding to the TmIG (400), (420), and (444) planes (JCPDS No. 23–0591), respectively. It proves that the TmIG film has a good crystalline structure with preferred orientation in [111] direction.

Given that the lattice constant of TmIG and sGGG are 12.324 and 12.480 Å, respectively, the TmIG films grown on the sGGG substrates suffer a tensile strain of about 1.265% [7,38]. Under such a strain state, the TmIG film with 10 nm thickness shows perpendicular magnetic anisotropy (PMA), as demonstrated by Fig. 1(e), which is consistent with previous reports [39–41]. The anomalous Hall resistance loops for the Hall bar with a stacking structure of TmIG/Pt are presented in Fig. 1(f) in which the linear normal Hall resistance has been subtracted. The saturation field for the TmIG (10)/Pt (5) sample is much smaller than that of TmIG (20)/Pt (5), indicating the PMA weakening with the TmIG thickness increasing due to the strain relaxation by a thick TmIG layer. Therefore, we employ the TmIG (10)/Pt (5) bilayer in the following transport measurements.

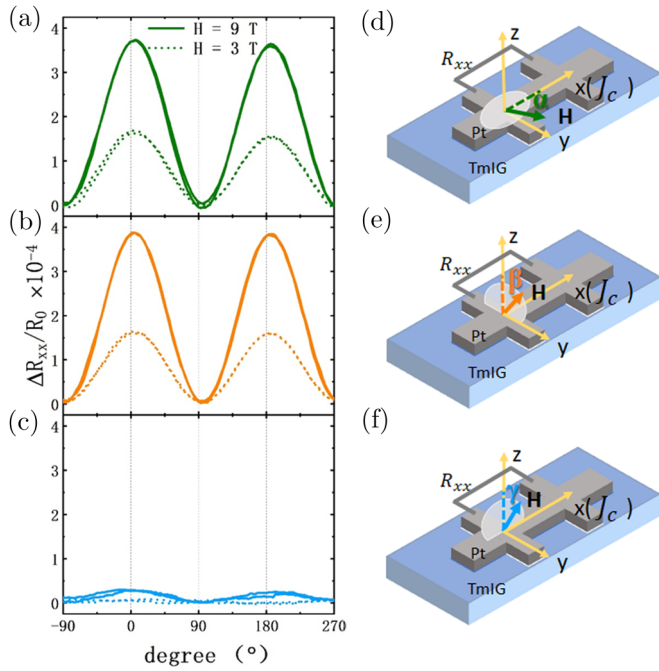


FIG. 2. (a)–(c) ADMR measurements for the TmIG (10)/Pt (5) sample under the magnetic fields of 3 T (dashed lines) and 9 T (solid lines) in three relevant magnetic field rotation planes ( $\alpha$ ,  $\beta$ ,  $\gamma$ ) at 300 K. (d)–(f) Sketches indicating the definition of the angles and the axes, corresponding to each ADMR measurement. The dashed lines represent the  $0^\circ$  angle.

To distinguish the contribution of different types of MR, we have carried out ADMR measurements in three rotation directions ( $\alpha$ ,  $\beta$ , and  $\gamma$ ) under 3 and 9 T respectively, and the results are presented in Fig. 2, together with each configuration scheme. The different kinds of MR are defined as  $MR(\alpha)$ ,  $MR(\beta)$  and  $MR(\gamma)$ , corresponding to the rotation planes of  $xy$ ,  $yz$ , and  $xz$ , respectively. According to Fig. 1(e), the magnetization of the TmIG layer is saturated and follows the direction of external magnetic field. The angular dependence of ADMR deviates less than  $10^\circ$ , which is caused by the system error from the instrument. As the SMR theory describes [11,12], there should be a large modulation with the  $\cos^2(\alpha, \beta)$  dependence and proportional to the external magnetic field for  $MR(\alpha, \beta)$ , while no clear signal could be observed for  $MR(\gamma)$ . Obviously, the curves in Figs. 2(a) and 2(b) agree with the theory of SHE and ISHE. However,  $MR(\gamma)$ , namely AMR, also exhibits a notable change under 9 T, although the magnitude is only one tenth of  $MR(\alpha, \beta)$ , which is interesting and needs more study in the future.

The interfacial effect of multilayer structures is significant to the transport properties of spintronic devices. Besides the bulklike AMR in the magnetized Pt caused by MPE, it is proved that AMR is also relevant with the ferromagnet/paramagnet interface due to the spin-dependent scattering [42,43]. To distinguish the AMR signal of interface with that of bulk, a Cu layer with different thickness is inserted between the TmIG and Pt layers, since Cu is an effective spacer layer to eliminate MPE due to its long spin diffusion length and good conductivity. We have measured the  $MR(\gamma)$  of TmIG (10)/Pt (5) and TmIG (10)/Cu (2, 4 and 6)/Pt (5) from 300 K down

to 1.8 K at 3 and 9 T, respectively. For clearness, we only show the  $MR(\gamma)$  curves for the TmIG/Pt and TmIG/Cu (4)/Pt samples obtained under 3 and 9 T at 1.8 K in Fig. 3(a). More  $MR(\gamma)$  curves for the TmIG/Pt and TmIG/Cu (2)/Pt samples are presented in Fig. S1 of the Supplemental Material [44]. We define  $\Delta MR(\gamma)$  as  $(R_\perp - R_\parallel)/R_\parallel$ , where  $R_\parallel$  and  $R_\perp$  are the longitudinal resistance when the magnetic field is parallel or perpendicular to the current. The  $\Delta MR(\gamma)$  changes with temperature for each sample can be obtained from the  $MR(\gamma)$  curves and are presented in Fig. 3(b). The error bars come from the maximum and minimum of  $(R_\perp - R_\parallel)/R_\parallel$  when the samples rotated from  $0^\circ$  to  $360^\circ$  and then back to  $0^\circ$ . When  $MR(\gamma)$  is insensitive to angle,  $\Delta MR(\gamma)$  is approximated to be zero. Obviously, under a large magnetic field of 9 T,  $\Delta MR(\gamma)$  of the TmIG/Pt sample changes dramatically from negative to positive when the temperature increases from 5 to 50 K and then decreases slowly when the temperature keeps increasing. While at a relatively small magnetic field of 3 T,  $\Delta MR(\gamma)$  increases from negative to nearly zero at 50 K and then can be approximated to be zero with the further increased temperature. On the contrary, the  $\Delta MR(\gamma)$  of the samples with a Cu spacer layer is always positive and gradually decreases to zero. Consistent with the TmIG/Pt sample, the  $\Delta MR(\gamma)$  obtained for each Cu-inserted sample also shows a dependence on the external magnetic field. It demonstrates that AMR can be maintained to higher temperatures under a larger magnetic field.

In the MI/non-magnetic metal structures, AMR might be ascribed to several effects including ordinary magnetoresistance (OMR), MPE, and spin-dependent scattering. Considering the obvious magnetic-field dependence and material correlation of  $\Delta MR(\gamma)$ , OMR should be a key factor for AMR. In a thin film of several nanometers, the motion of electrons in the  $z$  direction is partially confined, so the contribution of OMR to  $MR(\gamma)$  is mainly due to the shape anisotropy and becomes prominent under a large magnetic field [45]. In the Cu-inserted samples, the Cu layer has a shunting effect and a different OMR coefficient to Pt, which is a possible contribution to the  $MR(\gamma)$  variation among the samples with different stacking structures under the same magnetic field. However, OMR cannot result in the signal changes at low temperatures. Interestingly, the  $\Delta MR(\gamma)$  of TmIG/Pt at 9 T increases monotonically with temperature decreasing from 300 to 50 K, which is consistent with the temperature dependence of MPE. Nevertheless, the increasing  $\Delta MR(\gamma)$  should not be only attributed to MPE, because the  $\Delta MR(\gamma)$  measured at 3 T stays at zero in the same temperature region. And MPE should be independent of the external magnetic field as a kind of interfacial effect. Moreover, the  $\Delta MR(\gamma)$  of the Cu-inserted samples also increases with the decreasing temperature, but MPE should be eliminated in these samples. To further clarify the contribution of MPE, a control sample of sGGG/Pt (5) is studied and discussed in the Supplemental Material [44]. The temperature dependence of AMR can also be induced by spin-dependent scattering. At high temperatures, the spin-dependent effect is offset by spin-independent scattering, such as electron-phonon scattering, which decreases at low temperatures. Even though spin-dependent scattering cannot result in the signal changes of TmIG/Pt at low temperatures. Therefore, the dramatic change of  $\Delta MR(\gamma)$



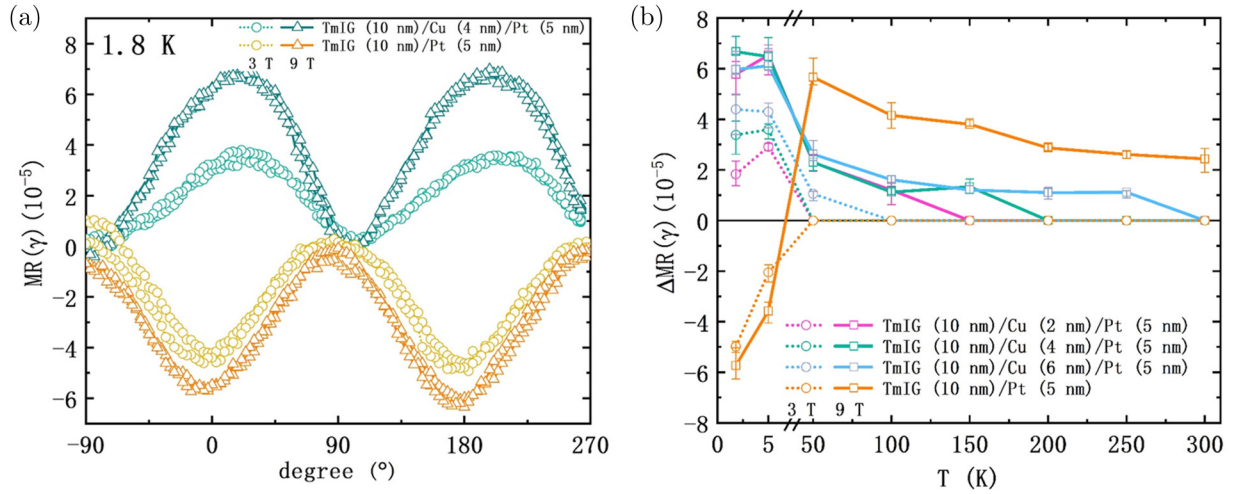


FIG. 3. (a)  $MR(\gamma)$  at 1.8 K for the samples of TmIG (10)/Pt (5) and TmIG (10)/Cu (4)/Pt (5) obtained at 3 and 9 T. (b) Temperature dependence of the  $\Delta MR(\gamma)$  defined as  $(R_{\perp} - R_{\parallel})/R_{\parallel}$ , where  $R_{\parallel}$  and  $R_{\perp}$  are the longitudinal resistances of the samples when the magnetic field is parallel or perpendicular to the current obtained at 3 T (dashed lines) and 9 T (solid lines). When  $MR(\gamma)$  is insensitive to angle,  $\Delta MR(\gamma)$  is approximated as zero.

below 50 K cannot be explained by traditional theories and must be caused by other effects.

Considering the low temperature and strong spin-orbit coupling in the ultrathin Pt films, the  $\Delta MR(\gamma)$  changes in these samples might be affected by WL or WAL. Since the AMR caused by OMR or the MPE-induced ordinary magnetism is quite small in the TmIG/Pt bilayer, the contribution of WAL or WL becomes significant in the AMR signals. And the quantum interference related correction on AMR is caused by the strong anisotropic inelastic field when a magnetic field is applied along the  $x$  and  $z$  axis, respectively [46]. To reveal the increasing influence of the quantum correction effect, the longitudinal resistance  $R_{xx}$  was measured versus temperature for the samples with and without the Cu spacer layer, together with that of a pure Pt layer, as shown in Fig. 4(a). With decreasing temperature,  $R_{xx}$  tends to be

stable, revealing the increasing phase coherence length  $l_{\phi}$ . And the normalized  $R_{xx}$  was calculated relative to the  $R_{xx}$  at 1.8 K, as shown in the inset of Fig. 4(a). Clearly,  $\Delta R_{xx}$  of the TmIG/Cu/Pt and sGGG/Pt samples are negative at extremely low temperatures, which may be related to the saturation of  $l_{\phi}$  or an increasing surface scattering [32,37]. Because  $\Delta R_{xx}$  of TmIG/Pt in Fig. 4(a) is positive in the whole temperature region, the destructive or constructive quantum interference between the time-reversed scattering closed loops may be significant enough to be observed in longitudinal resistance and consequently lead to the different tendencies of the  $\Delta R_{xx}$  curves at low temperature region. Moreover, the MR curves of sGGG/Pt in Fig. 4(b) show sharper cusps at the same temperature region. The sharper cusps are typical WAL characteristics, which agree with the dominated WAL in nonferromagnetic films. However, as TmIG is ferrimagnetic,

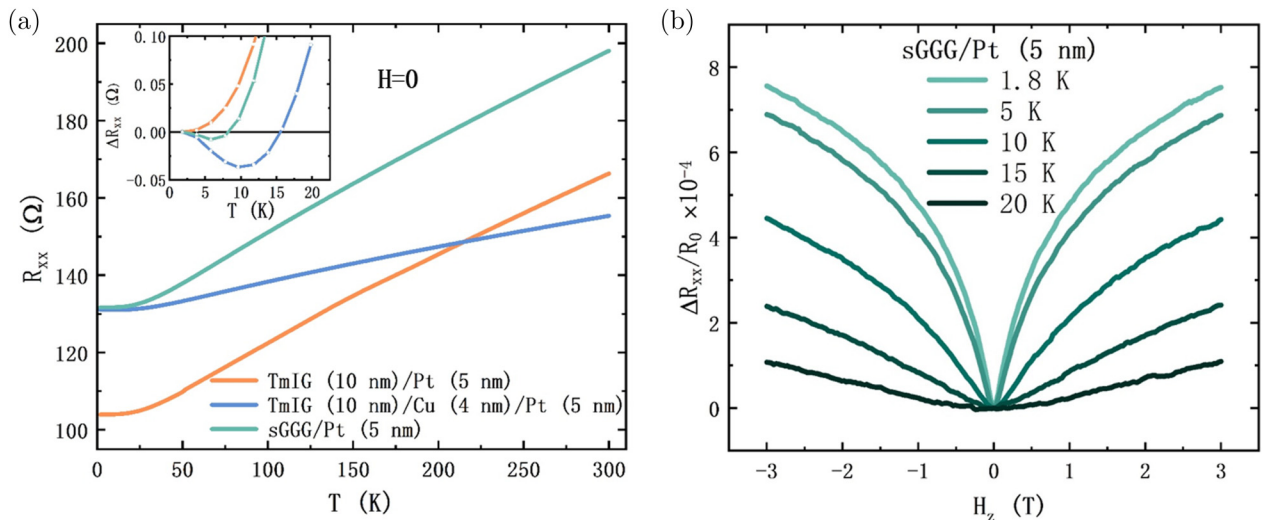


FIG. 4. (a) Temperature dependence of the longitudinal resistance  $R_{xx}$  for the three samples. The  $\Delta R_{xx}$  in the inset was calculated relative to  $R_{xx}$  at 1.8 K. (b) MR of the sGGG/Pt (5) sample measured at low temperature.

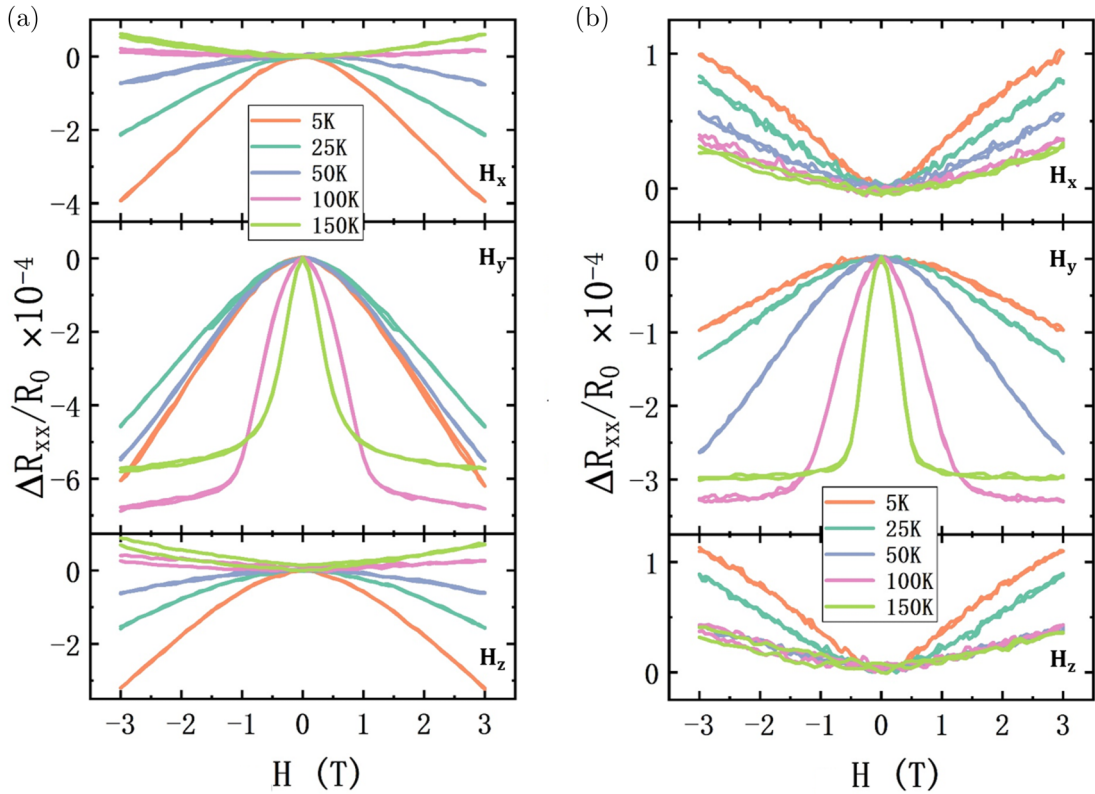


FIG. 5. MR results for the samples of (a) TmIG (10)/Pt (5) and (b) TmIG (10)/Cu (4)/Pt (5) obtained under magnetic fields along  $x$ ,  $y$ , and  $z$  axes.

a sizable MPE should exist at the TmIG/Pt interface, which is absent in the Cu inserted samples and pure Pt sample. In this case, the quantum correction on the conductance of the TmIG/Pt structure should be dominated by WL.

To further demonstrate the contribution of WL and WAL, we compare the MR results of TmIG/Pt and TmIG/Cu (4)/Pt in Fig. 5. When the magnetic field is along the  $x$  axis and the  $z$  axis, the MR of the TmIG/Pt sample becomes negative with the temperature decreasing to 50 K, which is typical of WL. In the TmIG/Cu (4)/Pt sample, the corresponding MR is positive over the whole temperature region and increases obviously at temperatures below 50 K due to WAL. When the magnetic field is applied along the  $y$  axis, the MR curves for both samples show similar trends, which are caused by SHE and related to the saturation field along the  $y$  axis. However, it is noticeable that, in TmIG/Pt, the MR at 5 K is more negative than that at 25 K, which should be attributed to WL. Furthermore, we have calculated a relative conductivity  $C = [R(B) - R(0)]/R^2(0)$  of the samples sGGG/Pt, TmIG/Pt, and TmIG/Cu (4)/Pt at 1.8 and 5 K when the magnetic field is along the  $z$  axis. The relative conductivity can be fitted approximately as a two-dimensional system proposed by the extended Hikami-Larkin-Nagaoka (HLN) formula [47,48],

$$C = \frac{R(B) - R(0)}{R^2(0)} = \frac{\alpha e^2}{2\pi^2 \hbar} \left[ \psi \left( \frac{1}{2} + \frac{1}{a\tau_\varepsilon} \right) - \ln \left( \frac{1}{a\tau_\varepsilon} \right) \right], \quad (1)$$

where  $a = 4DeB/\hbar$ ,  $D$  is the diffusion constant of the charge carriers,  $\psi$  is the digamma function, and  $\alpha$  is a coefficient

indicating the type of localization. The parameter  $\alpha$  in Eq. (1) depends on the relative magnitude of the various relaxation times  $\tau_{so}$ ,  $\tau_s$ , and  $\tau_\varepsilon$ , which represent spin-orbit, magnetic, and energy relaxation scattering, respectively. According to Refs. [46,47], if the spin-orbit interaction and magnetic scattering are weak ( $\tau_\varepsilon \ll \tau_{so}, \tau_s$ ), we have  $\alpha = -1$ . In this case, WL dominates and a negative temperature coefficient of resistance is accompanied by a negative magnetoresistance. However, if spin-orbit scattering dominates the inelastic and magnetic scattering processes ( $\tau_{so} \ll \tau_\varepsilon, \tau_s$ ), we have  $\alpha = 1/2$ , and WAL is dominant. The case  $\alpha = 0$  is given by the strong magnetic scattering in which WL and WAL disappear. The deviation of  $\alpha$  from  $-1$ ,  $0$ , or  $1/2$  can be interpreted as a crossover between the two states. As shown in Fig. 6, the relative conductivity of sGGG/Pt and TmIG/Cu (4)/Pt can be well fit by Eq. (1) with  $\alpha = 0.17$  and  $0.03$ , demonstrating a typical WAL behavior. For the TmIG/Pt sample, Eq. (1) fits the relative conductivity well with  $\alpha = -0.42$ , indicating a typical WL behavior. The relationship between  $\alpha$  and spin-orbit coupling has also been demonstrated in a Bi system in which  $\alpha$  was fit to be  $0.50 \pm 0.05$ , indicating a WAL characteristic [48]. It is well known that the spin-orbit coupling of Bi is stronger than that of Pt. Correspondingly, the  $\alpha$  of Pt in our study is smaller than that of Bi.

As described above, we have demonstrated the WL behavior in the TmIG/Pt sample. However, it is noteworthy that the TmIG/Pt sample do not satisfy the conditions of weak spin-orbit interaction and the magnetic scattering ( $\tau_\varepsilon \ll \tau_{so}, \tau_s$ ). It has been reported theoretically by Dugaev *et al.* [49] that the strong magnetic polarization in ferromagnetic materials

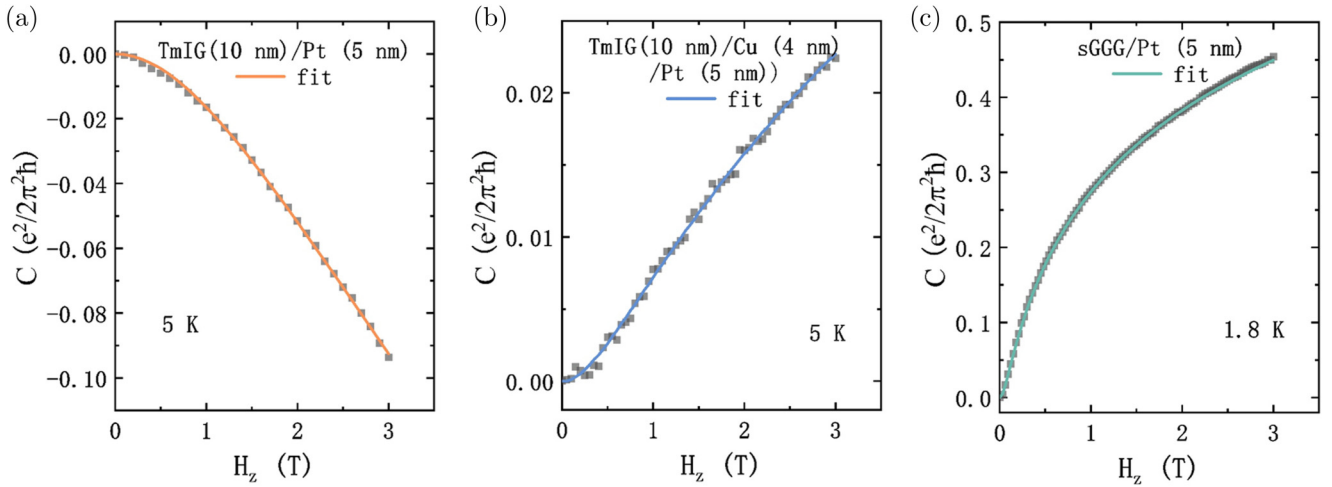


FIG. 6. The relative conductivity (black symbols) together with fitting curve for the samples of (a) sGGG/Pt (5), (b) TmIG (10)/Cu (4)/Pt, and (c) TmIG (10)/Pt (5).

excludes processes with the singlet Cooperon, which are responsible for the anti-localization in nonmagnetic materials with spin-orbit scattering. Considering the strong MPE in the TmIG/Pt sample, the Pt layer has not only strong bulk spin-orbit coupling but also interfacial magnetization at low temperatures, which is the reason why the localization corrections to conductivity lead to a negative MR in the TmIG/Pt sample. Yang *et al.* [37] also reported a pronounced WL that competes with the WAL in the YIG/Bi<sub>2</sub>Se<sub>3</sub> and TmIG/Bi<sub>2</sub>Se<sub>3</sub> bilayers, which was attributed to the time-reversal-symmetry breaking of topological surface states induced by MPE. Therefore, MPE plays an important role in magnetization and determines the contributions of WL or WAL. Besides, Kurzweil *et al.* [50] reported amorphous ultrathin films of Ni and Fe with extremely low Curie temperatures to study the conductivity of a single sample with or without ferromagnetism. The experimental results show that, in the paramagnetic phase of Ni and Fe films, the positive MR is governed by WAL, resulting from the strong Bychkov-Rashba spin-orbit scattering. However, in the ferromagnetic phase, the MR is negative due to the magnetism. In summary, our study

on the heterostructures TmIG/Pt, sGGG/Pt, and TmIG/Cu/Pt demonstrates the existence of the WL or WAL in the Pt films at low temperatures, and the dominant effect changes from WAL to WL due to the MPE-induced magnetism.

Finally, the correction on the  $\Delta MR(\gamma)$  at low temperatures is proved to be a kind of quantum correction related to localization. As the temperature dependence of resistance is another significant behavior of localization [30,31], the temperature coefficient of resistance (TCR) and  $\Delta MR(\gamma)$  for TmIG (10)/Pt (5) and TmIG/Cu (4)/Pt with a smaller temperature interval are compared in Fig. 7. Here, the TCR is defined as  $(1/R_1)(R_2 - R_1)/(T_2 - T_1)$  and calculated from Fig. 4(a). The  $\Delta MR(\gamma)$  curve of TmIG/Pt (or TmIG/Cu/Pt) decreases (increases) greatly from about 15 K (30 K) with decreasing temperature. Although the inflection points of  $\Delta MR(\gamma)$  appear at different temperatures, the TCR for the two samples are almost the same at  $5 \times 10^{-4} \text{ K}^{-1}$ . This consistency of TCR proves the same origin of the corrections, while the opposite temperature dependences of  $\Delta MR(\gamma)$  further demonstrate the different kinds of the corrections, which can be attributed to WL and WAL.

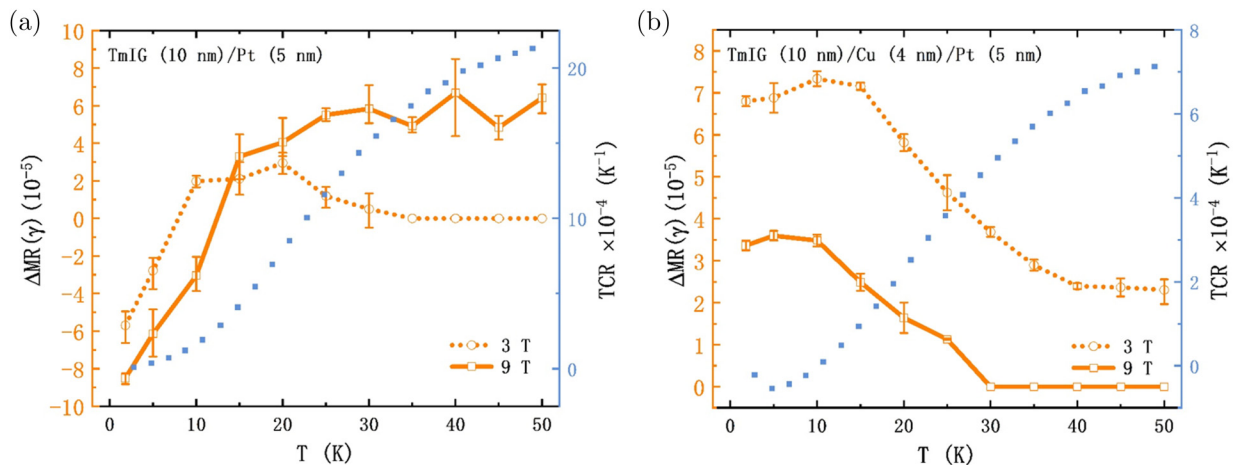


FIG. 7. Temperature dependence of  $\Delta MR(\gamma)$  and TCR for the samples of (a) TmIG (10)/Pt (5) and (b) TmIG (10)/Cu (4)/Pt (5).

WL and WAL dramatically correct the  $\Delta\text{MR}(\gamma)$  at low temperature region, indicating that the quantum interference plays an important role in the resistance and explains the novel AMR variation observed in the TmIG/Pt structure. According to previous studies [37,49,50], the WL or WAL corrections to conductivity can be affected by the directions of external field. Our study on the TmIG/Pt system further reveals the specific temperature and angular dependence. Inspired by the study on AMR, the quantum correction effect might bring other interesting MR signals having been ignored previously, which needs further investigation to reveal the true physical mechanism, especially at low temperatures.

#### IV. CONCLUSIONS

We have studied the quantum correction effect on the AMR in TmIG/Pt-based structures. By comparing the MR among the stacking structures sGGG/Pt, TmIG/Pt, and TmIG/Cu/Pt, we found that the OMR causes the difference of the MR between 3 and 9 T. The large spin-dependent scattering results in the increasing  $\Delta\text{MR}(\gamma)$  of both TmIG/Pt and TmIG/Cu/Pt

samples, with the temperature decreasing down to 50 K. At lower temperatures,  $\Delta\text{MR}(\gamma)$  further increases in the TmIG/Cu/Pt sample due to the WAL in the Pt layer. However, in the TmIG/Pt sample,  $\Delta\text{MR}(\gamma)$  decreases from positive to negative due to the WL in the magnetized Pt layer. Therefore, our study reveals the complicated origins of AMR under different application environments and proves the significant quantum correction effect at extremely low temperatures, which gives a deep insight into the behavior of AMR.

#### ACKNOWLEDGMENTS

We are grateful for the help of Z.F. Wang and H. Jia from the Analytical and Testing Center at TianGong University. This work was partially supported by the National Key Research and Development Program of China (2019YFB2005801), the Beijing Natural Science Foundation Key Program (Grant No. Z190007), and the National Natural Science Foundation of China (Grants No. 51731003, No. 52061135205, No. 51971024, No. 51971023, No. 51971027, and No. 51927802).

- 
- [1] R. D. M. P. E. Wigen and C. Jayaprakash, *J. Magn. Magn. Mater.* **84**, 237 (1990).
- [2] L. J. Cornelissen, J. Liu, R. A. Duine, J. B. Youssef, and B. J. van Wees, *Nat. Phys.* **11**, 1022 (2015).
- [3] Y. Kajiwara, K. Harii, S. Takahashi, J. Ohe, K. Uchida, M. Mizuguchi, H. Umezawa, H. Kawai, K. Ando, K. Takanashi *et al.*, *Nature (London)* **464**, 262 (2010).
- [4] S. P. Dalawai, A. B. Gadkari, and P. N. Vasambekar, *Rare Met.* **34**, 133 (2015).
- [5] C. O. Avci, E. Rosenberg, L. Caretta, F. Buttner, M. Mann, C. Marcus, D. Bono, C. A. Ross, and G. S. D. Beach, *Nat. Nanotechnol.* **14**, 561 (2019).
- [6] C. O. Avci, E. Rosenberg, M. Baumgartner, L. Beran, A. Quindeau, P. Gambardella, C. A. Ross, and G. S. D. Beach, *Appl. Phys. Lett.* **111**, 072406 (2017).
- [7] A. J. Lee, A. S. Ahmed, B. A. McCullian, S. Guo, M. Zhu, S. Yu, P. M. Woodward, J. Hwang, P. C. Hammel, and F. Yang, *Phys. Rev. Lett.* **124**, 257202 (2020).
- [8] J. E. Hirsch, *Phys. Rev. Lett.* **83**, 1834 (1999).
- [9] M. Isasa, E. Villamor, L. E. Hueso, M. Gradhand, and F. Casanova, *Phys. Rev. B* **91**, 024402 (2015).
- [10] M. Morota, Y. Niimi, K. Ohnishi, D. H. Wei, T. Tanaka, H. Kontani, T. Kimura, and Y. Otani, *Phys. Rev. B* **83**, 174405 (2011).
- [11] M. Althammer, S. Meyer, H. Nakayama, M. Schreier, S. Altmannshofer, M. Weiler, H. Huebl, S. Geprags, M. Opel, R. Gross *et al.*, *Phys. Rev. B* **87**, 224401 (2013).
- [12] Y.-T. Chen, S. Takahashi, H. Nakayama, M. Althammer, S. T. B. Goennenwein, E. Saitoh, and G. E. W. Bauer, *Phys. Rev. B* **87**, 144411 (2013).
- [13] C. Hahn, G. de Loubens, O. Klein, M. Viret, V. V. Naletov, and J. Ben Youssef, *Phys. Rev. B* **87**, 174417 (2013).
- [14] M. Isasa, A. Bedoya-Pinto, S. Véléz, F. Golmar, F. Sánchez, L. E. Hueso, J. Fontcuberta, and F. Casanova, *Appl. Phys. Lett.* **105**, 142402 (2014).
- [15] H. Nakayama, M. Althammer, Y. T. Chen, K. Uchida, Y. Kajiwara, D. Kikuchi, T. Ohtani, S. Geprags, M. Opel, S. Takahashi *et al.*, *Phys. Rev. Lett.* **110**, 206601 (2013).
- [16] N. Vlietstra, J. Shan, V. Castel, J. Ben Youssef, G. E. W. Bauer, and B. J. van Wees, *Appl. Phys. Lett.* **103**, 032401 (2013).
- [17] N. Vlietstra, J. Shan, V. Castel, B. J. van Wees, and J. Ben Youssef, *Phys. Rev. B* **87**, 184421 (2013).
- [18] N. Vlietstra, J. Shan, B. J. van Wees, M. Isasa, F. Casanova, and J. Ben Youssef, *Phys. Rev. B* **90**, 174436 (2014).
- [19] I. Campbell, A. Fert, and O. Jaoul, *J. Phys. C: Solid State Phys.* **3**, S95 (1970).
- [20] T. R. McGuire and R. I. Potter, *IEEE Trans. Magn.* **11**, 1018 (1975).
- [21] W. Thomson, *Proc. R. Soc. Lond.* **8**, 546 (1857).
- [22] S. Y. Huang, X. Fan, D. Qu, Y. P. Chen, W. G. Wang, J. Wu, T. Y. Chen, J. Q. Xiao, and C. L. Chien, *Phys. Rev. Lett.* **109**, 107204 (2012).
- [23] T. Lin, C. Tang, H. M. Alyahyaei, and J. Shi, *Phys. Rev. Lett.* **113**, 037203 (2014).
- [24] T. Lin, C. Tang, and J. Shi, *Appl. Phys. Lett.* **103**, 132407 (2013).
- [25] Y. M. Lu, J. W. Cai, S. Y. Huang, D. Qu, B. F. Miao, and C. L. Chien, *Phys. Rev. B* **87**, 220409(R) (2013).
- [26] B. F. Miao, S. Y. Huang, D. Qu, and C. L. Chien, *Phys. Rev. Lett.* **112**, 236601 (2014).
- [27] Y. Yang, B. Wu, K. Yao, S. Shannigrahi, B. Zong, and Y. Wu, *J. Appl. Phys.* **115**, 17C509 (2014).
- [28] S. Velez, V. N. Golovach, A. Bedoya-Pinto, M. Isasa, E. Sagasta, M. Abadia, C. Rogero, L. E. Hueso, F. S. Bergeret, and F. Casanova, *Phys. Rev. Lett.* **116**, 016603 (2016).
- [29] G. Bergmann, *Phys. Rep.* **107**, 1 (1984).
- [30] P. A. Lee and T. V. Ramakrishnan, *Rev. Mod. Phys.* **57**, 287 (1985).
- [31] S.-I. Kobayashi and F. Komori, *Prog. Theor. Phys. Suppl.* **84**, 224 (1985).



- [32] J. J. Lin and J. P. Bird, *J. Phys.: Condens. Matter* **14**, R501 (2002).
- [33] B. Kramer, G. Bergmann, and Y. Bruynseraede, *Localization, Interaction, and Transport Phenomena: Proceedings of the International Conference, August 23–28, 1984 Braunschweig, Fed. Rep. of Germany* (Springer Science & Business Media, Berlin, Heidelberg, 2012), Vol. 61.
- [34] B. Kramer and A. MacKinnon, *Rep. Prog. Phys.* **56**, 1469 (1993).
- [35] M. Lang, L. He, X. Kou, P. Upadhyaya, Y. Fan, H. Chu, Y. Jiang, J. H. Bardarson, W. Jiang, E. S. Choi *et al.*, *Nano Lett.* **13**, 48 (2013).
- [36] M. Liu, J. Zhang, C. Z. Chang, Z. Zhang, X. Feng, K. Li, K. He, L. L. Wang, X. Chen, X. Dai *et al.*, *Phys. Rev. Lett.* **108**, 036805 (2012).
- [37] S. R. Yang, Y. T. Fanchiang, C. C. Chen, C. C. Tseng, Y. C. Liu, M. X. Guo, M. Hong, S. F. Lee, and J. Kwo, *Phys. Rev. B* **100**, 045138 (2019).
- [38] A. S. Ahmed, A. J. Lee, N. Bagues, B. A. McCullian, A. M. A. Thabt, A. Perrine, P. K. Wu, J. R. Rowland, M. Randeria, P. C. Hammel *et al.*, *Nano Lett.* **19**, 5683 (2019).
- [39] M. Kubota, A. Tsukazaki, F. Kagawa, K. Shibuya, Y. Tokunaga, M. Kawasaki, and Y. Tokura, *Appl. Phys. Express* **5**, 103002 (2012).
- [40] O. Ciubotariu, A. Semisalova, K. Lenz, and M. Albrecht, *Sci. Rep.* **9**, 17474 (2019).
- [41] S. Xia, S. Zhang, Z. Luan, L. Zhou, J. Liang, G. Liu, B. Yang, H. Yang, R. Liu, and D. Wu, *Appl. Phys. Lett.* **116**, 052404 (2020).
- [42] A. Kobs, S. Hesse, W. Kreuzpaintner, G. Winkler, D. Lott, P. Weinberger, A. Schreyer, and H. P. Oepen, *Phys. Rev. Lett.* **106**, 217207 (2011).
- [43] A. Kobs and H. P. Oepen, *Phys. Rev. B* **93**, 014426 (2016).
- [44] See Supplemental Material at <http://link.aps.org/supplemental/10.1103/PhysRevB.105.184428> for more test results and detailed discussion.
- [45] L. Baldrati, A. Ross, T. Niizeki, C. Schneider, R. Ramos, J. Cramer, O. Gomonay, M. Filianina, T. Savchenko, D. Heinze *et al.*, *Phys. Rev. B* **98**, 024422 (2018).
- [46] S. Sangiao, N. Marcano, J. Fan, L. Morellón, M. R. Ibarra, and J. M. De Teresa, *Europhys. Lett.* **95**, 37002 (2011).
- [47] S. Hikami, A. I. Larkin, and Y. Nagaoka, *Prog. Theor. Phys.* **63**, 707 (1980).
- [48] P. H. Woerlee, G. C. Verkade, and A. G. M. Jansen, *J. Phys. C: Solid State Phys.* **16**, 3011 (1983).
- [49] V. K. Dugaev, P. Bruno, and J. Barnaś, *Phys. Rev. B* **64**, 144423 (2001).
- [50] N. Kurzweil, E. Kogan, and A. Frydman, *Phys. Rev. B* **82**, 235104 (2010).